SAND2022-1489J

The influence of surface impurities on photoelectric currents driven by intense soft x-rays

N. A. Roberds[a)]
Sandia National Laboratories, PO Box 5800, Albquerque, NM 87185, USA

(Dated: 1 February 2022)

In an x-ray driven cavity experiment, an intense flux of soft x-rays on the emitting surface produces significant emission of photoelectrons having several kiloelectronvolts of kinetic energy. At the same time, rapid heating of the emitting surface occurs, resulting in the release of adsorbed surface impurities and subsequent formation of an impurity plasma. This numerical study explores a simple model for the photoelectric currents and the impurity plasma. Attention is given to the effect of varying the composition of the impurity plasma. The presence of protons or hydrogen molecular ions leads to a substantially enhanced cavity current, while heavier plasma ions are seen to have a limited effect on the cavity current due to their lower mobility. Additionally, it is demonstrated that an additional peak in the current waveform can appear due to the impurity plasma. A correlation between the impurity plasma composition and the timing of this peak is elucidated.

I. INTRODUCTION

A recent series of experiments at the Z generator investigated the electrical currents induced in cavities which are exposed to intense soft x-rays with energies on the order of 1-10 kiloelectronvolts (keV).[1,2] The cavity geometry is cylindrically symmetric and all cavity surfaces are electrically conductive; there is continuous electrical contact across the entire cavity. On the top of the cavity is a circular window with radius $r = 20$ mm. The window is semi-transparent to x-rays, electrically conductive and also absorbs incident electrons. X-ray energy from a nearby Z-pinch wire array passes through the window to reach the gold-plated emitting surface on the bottom of the cavity.

Due to the large atomic number of gold, the emitting surface has a relatively high quantum yield for soft x-rays. When the emitter is illuminated by soft x-rays, fast photoelectrons having several keV of kinetic energy are emitted. The cavity includes a B-dot sensor to measure the return current from the top electron absorber to the bottom emitter. Given a sufficiently intense x-ray pulse, the electric current traversing the cavity gap is limited by the space charge barrier. In this case, the concentration of negative space charge above the emitter will electrostatically repulse many of the emitted electrons back into the emitter. The situation is similar to that in the analysis presented by Jaffé.[3] Jaffé considered the space charge limiting of a beam of monoenergetically emitted electrons traversing the gap between two grounded, parallel planes. More recently, Luginsland et al. considered a two-dimensional, monoenergetically emitted beam of electrons which transits a grounded cavity.[4] They found that, if the beam is turned on very quickly, electromagnetic induction can affect the virtual cathode formation and subsequent steady state behavior.

This study examines the effect of impurity plasma on the photoelectric current. In a typical shot, the gold surface absorbs around 15 $\mathrm{kJ/m^2}$ of x-ray energy over a 30 ns interval, with most of the energy deposition occurring between $t = 3$ to 4 ns. This rapidly heats the emitting surface and the inventory of adsorbed impurities is released from the surface by thermal desorption early in the shot. Some fraction of the desorbed impurity gas will be ionized by impact with photoelectrons or by other mechanisms.

Section II describes the cavity model and its approximations. Quantitative agreement between model solutions and any experiment is not expected. Rather, the intent is to gain insight into the effect of the impurity plasma and the significance of its composition. It should be noted that the importance of the conditioning of electrode surfaces is well known for high power vacuum electronics.[5–8] Unlike the x-ray driven cavity, in which all surfaces are electrically grounded, in these devices a large potential difference may exist across the top (say anode) and bottom (say cathode) electrodes, and impurities may come off both. In high power vacuum electronics, the electrode impurity plasmas have been observed to expand across the anode-cathode gap.[9,10] The diode impedance drops as the electrodes are bridged by an electrically conductive plasma. An anode plasma can serve as a space charge limited emitter of ions. When space charge limited emission of protons from the anode is modeled, the beam current of a 1D electron diode in steady state operation is increased by a factor of 1.86 over the non-relativistic Child-Langmuir space charge limit.[11,12] In the context of high power vacuum electronics, it is well established that the population of protons and hydrogen molecular ions in the impurity plasma are of elevated importance in high power, short pulse applications compared to the populations of heavier ions.[13] Weber et al. found that conditioning a tantalum anode with a preheating pulse just before energizing the anode-cathode gap significantly enhanced the performance of a high power diode.[14] They noted that, although some quantity of tantalum would be vaporized during the main discharge, the large atomic mass of tantalum ions ensures that they would have a minimal effect during the short 100 ns pulse compared to impurity ions. In the x-ray driven cavity, heavy gold ions resulting from ablation of the emitter surface are expected.

Section III presents the calculation results. The elevated importance of impurity plasma ions with a low molecular

[a)]Electronic mail: nroberd@sandia.gov

Sandia National Laboratories is a multimission laboratory managed and operated by National Technology & Engineering Solutions of Sandia, LLC, a wholly owned subsidiary of Honeywell International Inc., for the U.S. Department of Energy's National Nuclear Security Administration under contract DE-NA0003525.

mass is demonstrated with a sequence of calculations which vary the relative quantity of light impurity ions in the injected plasma. Calculations with only massive impurity ions confirm that ions with a high molecular mass take too long to transit the cavity gap to have a significant impact on the maximum cavity current in the short pulse device under consideration. Additionally, the results give an intuition on how a population of impurity ions, having a given molecular mass, will affect the photocurrent waveform shape.

Section IV presents a summary and discussion. Avenues for future work are suggested, especially regarding the determination of the important physical processes occurring on the emitter surface and self-consistent calculation of the impurity plasma formation.

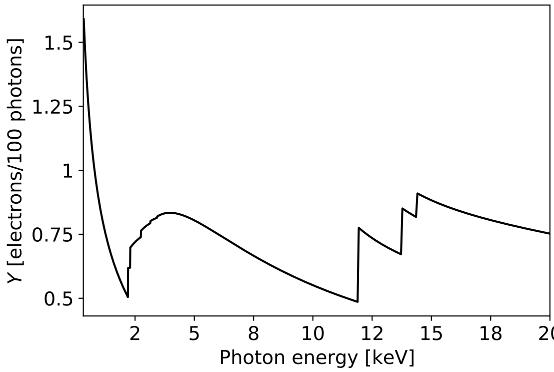

FIG. 1. A plot of the approximate quantum yield for gold, $Y(h\nu)$, for soft x-ray photons up to 20 keV. The N, M and L shell primary photoelectrons and the L shell Auger photoelectrons are accounted for in this model.

II. PROBLEM SPECIFICATION

A 1D-3V, electrostatic, particle-in-cell (PIC) model is used in this work. Still, it is convenient to use the EMPIRE particle-in-cell (PIC) code, which is capable of carrying out both electrostatic and electromagnetic simulations in two- and three-dimensional spaces using a variety of mesh topologies. The implementation and numerical methods of EMPIRE have been described by Bettencourt et al.[15] A periodic two-dimensional grid, having rectangular grid elements, is used. The grid has a uniform 2 μm spacing in the non-periodic (x) direction and is two elements wide in the periodic direction. The width in the periodic direction is 13 μm, so computational particles can be considered to be charge sheets which are represented with an infinite number of line charges extending along the periodic direction. With these parameters, the electric field in the periodic direction was confirmed to be negligible with a typical magnitude around 10^{-8} V/m. Time step size is set to correspond to a Courant-Friedrichs-Lewy (CFL) number of unity for 10 keV electrons.

The electrostatic boundary conditions set the electric potentials of the emitting surface at $x = 0$ and the top surface at $x = d$ to ground. Absorbing particle boundary conditions are applied to both surfaces; all computational particles are absorbed when they are incident on cavity surfaces. Photoelectrons and impurity plasma constituents are injected normally from the plane which represents the heated photoelectric emitter. X-rays are considered to be normally incident on the top of the cavity, and the interaction between the x-rays and the semi-transparent window is considered to be negligible although this is acknowledged to be a simplifying approximation within the model. Therefore, an area πr^2 of the emitter can be considered to be illuminated by x-rays. For convenience then, the electric currents reported in section III are the 1D current densities scaled by an areal factor of πr^2.

In these calculations the emitter surface is irradiated with a blackbody spectrum,

$$B(h\nu,T) = \left(\frac{15h(h\nu)^3}{k_\mathrm{B}^4\pi^4T^4}\right)\frac{1}{\exp\left(\frac{h\nu}{k_BT}\right)-1}, \tag{1}$$

where k_B is the Boltzmann constant and h is Planck's constant. The spectrum temperature is chosen to be $T = 1.6$ keV so that the average photon energy is 6 keV. The x-ray fluence is $\varphi = 15$ kJ/m^2, so the energy deposited in the gold emitter is then 18.85 J. The pulse shape of the x-ray intensity is given by a time resolved measurement of the normalized x-ray intensity generated by a wire array load during shot Z2234 on the Z generator.[16] With these parameters, the computed cavity current mimics the experimentally measured current for shot Z2234 quite well. Note that the x-ray pulse has two peaks: one at $t = 5$ ns and a smaller peak at $t = 25$ ns.

The approximate quantum yield for gold, $Y(h\nu)$, was computed using the procedure outlined by Burke.[17,18] The N, M and L shell primary photoelectrons and L shell Auger photoelectrons are accounted for. The quantum yield $Y(h\nu)$ is plotted in Fig. 1. This procedure also yields the photoelectron energy distribution (EEDF), $dY/dE(E,h\nu)$. The normalization of the EEDF is such that,

$$Y(h\nu) = \int \frac{dY}{dE}(E,h\nu)\,dE, \tag{2}$$

where $h\nu$ is the energy of an incident photon and E is the energy of an emitted photoelectron. Calculation of the primary photoelectron yields requires information about the discontinuities in the x-ray mass absorption coefficient at absorption edges. That information was obtained from the tabulations provided by Biggs and Lighthill.[19] The average fluorescence yield for the L shells tabulated by Hubbell et al. were used to compute the Auger photoelectron yield.[20]

The EEDF for high energy photoelectrons driven off a gold surface by this x-ray spectrum can be computed by a convolution of the monoenergetic EEDF with the blackbody spectrum,

$$\frac{dY}{dE}(E) = \int \frac{dY}{dE}(E,h\nu)B(h\nu,T)\,d(h\nu). \tag{3}$$

To provide insight into the form of $dY/dE(E)$, Fig. 2(a) plots $dY/dE(E,h\nu)$ for several values of $h\nu$ as well as $B(h\nu,T)$.

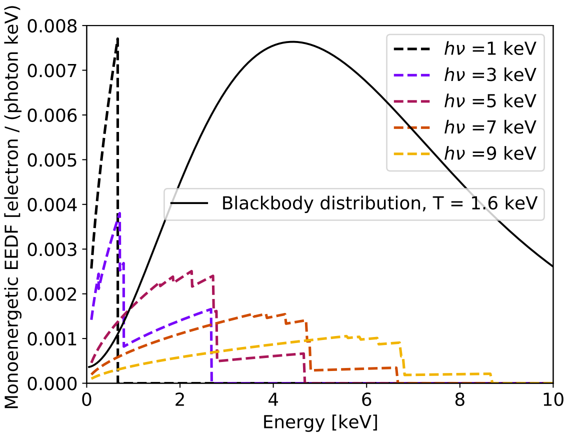

(a)

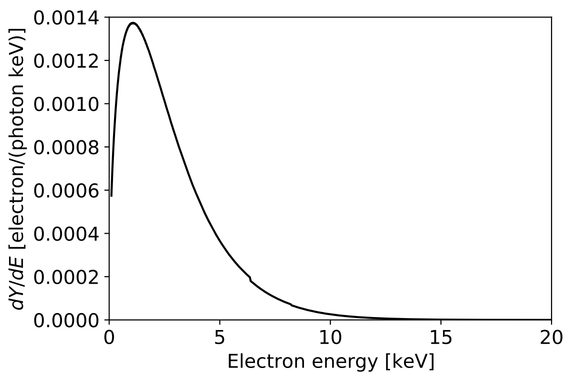

(b)

FIG. 2. Panel (a) shows the monoenergetic EEDFs, $dY/dE(E,h\nu)$, for several photon energies as well as the x-ray blackbody spectrum used in this calculation. The blackbody spectrum is plotted in normalized units. The plots of these quantities provides insight into the form of the EEDF for the photoelectrons used in this calculation. Shown in (b) is the approximate EEDF, $dY/dE(E)$, for photoelectrons emitted from a gold surface that is driven by a blackbody soft x-ray spectrum corresponding to a temperature of $T = 1.6$ keV. The average photoelectron energy is $E_0 = 2.8$ keV. This EEDF is obtained by convolving the monoenergetic EEDF with the x-ray spectrum.

The form of the monoenergetic EEDFs shown in Fig. 2(a) are reflective of processes involved in photoelectron production. Especially, photoelectrons are created some distance under the surface and then lose energy as they scatter towards the surface. A plot of $dY/dE(E)$ is shown in Fig. 2(b). The average energy for primary and Auger photoelectrons is $E_0 = 2.8$ keV. The quantum yield for these high energy photoelectrons, $Y = 5.2\times10^{-3}$, can then be obtained by integrating Eq. 3.

Besides these high energy primary photoelectrons and Auger electrons, there will be a significant population of low energy secondary photoelectrons, also referred to as delta rays or *knock-on* electrons. Typically, for keV soft x-rays, low energy secondary photoelectrons account for between 50 to 90% of the total number of emitted photoelectrons.[21,22] To account for secondary photoelectrons, a beam of electrons is injected from the emitting surface with temperature $T = 10$ eV. The emitted current density is set equal to that of the high energy photoelectrons. Including secondary photoelectron emission, the total quantum yield of the present model is 1.04×10^{-2}. Another consideration is that the emitter surface is made of some substrate covered with a thin plating of gold. For the purpose of computing photoelectric emissions due to incident soft x-rays, a gold coating thicker than about 10 nm can be considered be to a solid gold surface.[22]

In this photoelectron emission model, high energy photoelectron emission velocities are normal to the emitting surface, although it is recognized that this simplifying assumption is not physically accurate. The ITS code, for example, is capable of computing a more realistic emission model.[23]

Impurity plasma is injected from the emitting surface at a constant rate after the surface temperature would be above 760 K, at $t_0 = 3.8$ ns. The impurity plasma electrons and ions are injected with a temperature $T = 1$ eV. The start time of plasma injection, t_0, in these simulations was informed by a calculation of the emitter surface temperature and impurity desorption. The surface temperature was computed using a simple model for x-ray heating. The emitter was considered to be a semi-infinite slab having the thermal conductivity and heat capacity of room temperature gold. A detailed description of the method used to compute the surface temperature was given by Roberds et al.[24] The volumetric heating profile was computed according to the mass absorption coefficient for gold as given by Biggs and Lighthill and the assumed Plankian x-ray spectrum.[19] X-rays are assumed to deposit all of their energy as thermal energy upon absorption; all other processes have been neglected.

The impurity desorption flux is taken to be given by the Polanyi-Wigner equation,[25]

$$\Gamma(t) = \kappa\theta(t)\exp\left(\frac{-E_a}{k_B T(t)}\right) \tag{4}$$

$$\dot{\theta}(t) = -\Gamma(t), \tag{5}$$

where here T is the surface temperature, $\kappa = 10^{13}$ s^{-1} is a frequency factor and $E_a = 0.5$ eV is the desorption activation energy. The adsorbate surface density, θ, decreases in time with the desorption rate and the initial adsorbate density is $\theta(t=0) = 10^{19}$ m^{-2}. The computed surface temperature and fraction of desorbed impurities are plotted in Fig. 3. When the surface temperature reaches approximately 760 K, which occurs at 3.8 ns, approximately half of the impurities have been desorbed. The start time of plasma injection from the emitting surface is therefore taken to be $t_0 = 3.8$ ns. The inclusion of heat conduction in the temperature calculation has a significant effect on the result; the decrease in temperature starting at 7 ns is due to heat conduction. A more sophisticated model for the surface temperature and x-ray heating source does affect the computed temperature, but would unnecessarily complicate the analysis in what follows. Note that given the present model, nearly all of the impurities have desorbed before the melting temperature, about 1300 K, is reached. It should be emphasized that Eq. 4 does not prescribe an injection flux in

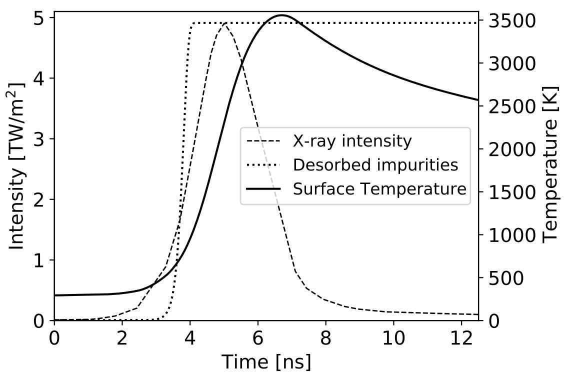

FIG. 3. Computed temperature of a gold surface heated by a 15 kJ/m^2 x-ray pulse. Room temperature thermal properties for gold were assumed, and a simple model for the volumetric heating profile was used. The rate of impurity desorption is given by the Polanyi-Wigner equation. This calculation informs the start of impurity plasma injection in the x-ray driven cavity simulations. Approximately half of the impurities have desorbed at $t = 3.8$ ns.

the simulations. This model for desorption is merely used to determine a start time for impurity plasma injection which proceeds at a constant rate.

The injected impurity plasma is composed of heavy ions and light ions (as well as plasma electrons). Two types of light ions, denoted H+ and H_2+, will be considered. The H+ ions have the mass of a proton. An H_2+ ion has twice the mass of an H+ ion. The heavy ions, H_2O+, have 18 times the mass of an H+ ion. The injected plasma composition is characterized by the parameter H_{frac}, which is the fraction of plasma ions which are light ions. H_{frac} is varied to study the effect of plasma composition on the cavity current.

The model described in this section intends to capture the essential phenomena of interest: transport of the impurity ions into the cavity due to the electron space charge field and the subsequent reduction of the space charge barrier which is associated with an enhanced electron beam current. Here, the space charge barrier is defined to be the minimum value of the electric potential times the charge of an electron. It provides a measure of the strength of the cavity current limiting effect and it will tend to increase as the emitted photocurrent increases. Emitted photoelectrons will be reflected back towards the emitting surface if the potential barrier exceeds the kinetic energy of emitted electrons; a virtual cathode forms in this situation.

III. RESULTS

Several cases characterized by the parameter H_{frac} and by the type of light impurity ions are considered in this section. In the reference case there is no impurity ion emission; only the emission of photoelectrons takes place in the reference case. In all other cases, impurity plasma ions are injected at a rate 3.8×10^{15} m^{-2}ns^{-1} from t_0 until the end of the run at $t = 30$ ns. Note that currents reported in this section have been scaled by a factor of πr^2 since the 1D calculation result is a current density with units A/m^2. Although an electrostatic treatment is used for this problem, the displacement current is significant and is included in the reported cavity current. The reported cavity currents are therefore equivalent to those given by the Shockley-Ramo theorem (within the error associated with computing the time rate of the electric field).[26] In this section, the reported currents result from applying a 4$^{\text{th}}$ order low pass Butterworth filter, with a 10 GHz cutoff, to the current output by the simulation.[27] Filtering is used so that the results are easier to interpret. Without any filtering or time averaging, the instantaneously measured currents are quite noisy.

Results for the reference case and the case which includes emission of only heavy impurity ions H_2O+ ($H_{\text{frac}} = 0$) are shown in Fig. 4. There are two peaks in the cavity current corresponding to the two maxima in the x-ray intensity. The cavity current is strongly limited by the space charge barrier throughout the pulse for both the reference case and the $H_{\text{frac}} = 0$ case; cavity currents remain significantly below the emitted photocurrent as shown in Fig. 4(a). While the maximum emitted photoelectron current is 5.4 kA for high energy photoelectrons, the peak cavity current for both cases is 96 A at $t = 5$ ns. The space charge barriers are shown in Fig. 4(b). The peak space charge barrier value is 8.5 keV for both the reference case and $H_{\text{frac}} = 0$. Note that the current associated with the fraction (2%) of photoelectron emissions having an energy above 8.5 keV is 110 A during peak photoelectron emission. This is quite close, within 15%, to the computed peak cavity current of 96 A.

The $H_{\text{frac}} = 0$ cavity current steadily increases relative to the reference case after the first current peak at $t = 5$ ns. The effect of the impurity ions on the cavity current can be understood in terms of their effect on the space charge barrier. A lowering of the potential barrier, due to an introduction of positively charged ions, results in an increased current. The evolution of ion and electron densities is of interest and this is plotted in Fig. 4(c) for the $H_{\text{frac}} = 0$ case. A quasi-neutral plasma forms near the emitting surface and rapidly expands. In the interval from $t = 8$ to 10 ns, the expansion proceeds at an average speed 280 mm/μs. The expansion of the plasma effectively shortens the electrode gap width, since the electric field is roughly zero in the plasma region and no space charge limiting fields can set up there. Late in the pulse, the expansion of the plasma has significantly shortened the effective gap width and the cavity current is increased compared to the reference case.

The plasma expansion is driven by the acceleration of the ions due to the electron-space-charge electric field. This was determined by considering a problem similar to the case $H_{\text{frac}} = 0$, but which omits the emission of high energy electrons. It was seen that, when there is no emission of the high energy photoelectrons to drive a strong electric field in the cavity, the plasma expansion occurs much slower. Also note that the ions lead the plasma electrons in the expansion, so that there is a layer of ion space charge at the expansion front. The electron density in the transition between the quasi-neutral plasma and the ion layer is approximately consistent with the

Boltzmann relation,

$$n_e(x) = n_0 \exp\left(\frac{\phi(x) - \phi_0}{T_e}\right), \tag{6}$$

where n_0 and T_e are the electron density and temperature (in eV) in the quasi-neutral plasma, $\phi(x)$ is the electric potential and ϕ_0 is the electric potential in the plasma. Since short-range collisions are not modeled and the grid resolves the Debye length, T_e is determined by the injection temperature of low energy electrons.

When a population of light impurity ions are injected along with the heavy impurity ions, the results are qualitatively different. Results for cases including light impurity ions of type H+ are shown in Fig. 5. These cases exhibit a peak in the cavity current at around $t = 10$ ns, while for the reference and $H_{\mathrm{frac}} = 0$ cases the peak is at $t = 5$ ns. For $H_{\mathrm{frac}} = 1$, a quasi-neutral plasma fills the domain so that space charge fields are suppressed; it can be seen in Fig. 5(b) that the space charge barrier is zero after $t = 10$ ns. For $H_{\mathrm{frac}} = 0.05$ and $H_{\mathrm{frac}} = 0.25$, a minimum in the space charge barrier occurs when the cavity current peaks at $t = 10$ ns. Fig. 5(c) shows the evolution of the electron and ion densities for the $H_{\mathrm{frac}} = 0.25$ case. For all instants in time shown, there are two high ion density regions separated by a rarefied region. The dense region closest $x = 0$ is predominately filled with H_2O+ ions while the region closest $x = d$ contains only H+ ions. This can be explained in terms of the time history of the electric field and the difference in ion mass between H+ and H_2O+: light H+ ions are drawn from the plasma near $x = 0$ by the electric field. The H+ ions are rapidly accelerated across the gap. The peak in the cavity current at $t = 10$ ns approximately coincides with the light ions reaching the top of the cavity at $x = d$.

Note that, for $H_{\mathrm{frac}} = 0.25$, the plasma expansion proceeds more slowly compared to $H_{\mathrm{frac}} = 0$. In the interval from $t = 8$ to 10 ns, the expansion proceeds at an average speed 220 mm$/\mu$s, approximately 15% slower than $H_{\mathrm{frac}} = 0$. Indeed, the electric field at the expansion front is stronger for the $H_{\mathrm{frac}} = 0$ case over this interval.

If the more massive H_2+ light impurity ions are injected instead of H+, neutralization of the space charge barrier occurs more slowly due to the longer transit time of the heavier ions. Fig. 6 shows the cavity current for two cases, one with light impurity ions of type H+ and the other with H_2+. Both cases are $H_{\mathrm{frac}} = 0.05$. For H_2+, the cavity current peak and the minimum in the space charge barrier occur about 2.5 ns later than for H+. This is remarkably close to the slow down of 2.6 ns that is consistent with slowing due to the factor of 2 difference in mass between the ion types given static and uniform electric fields.

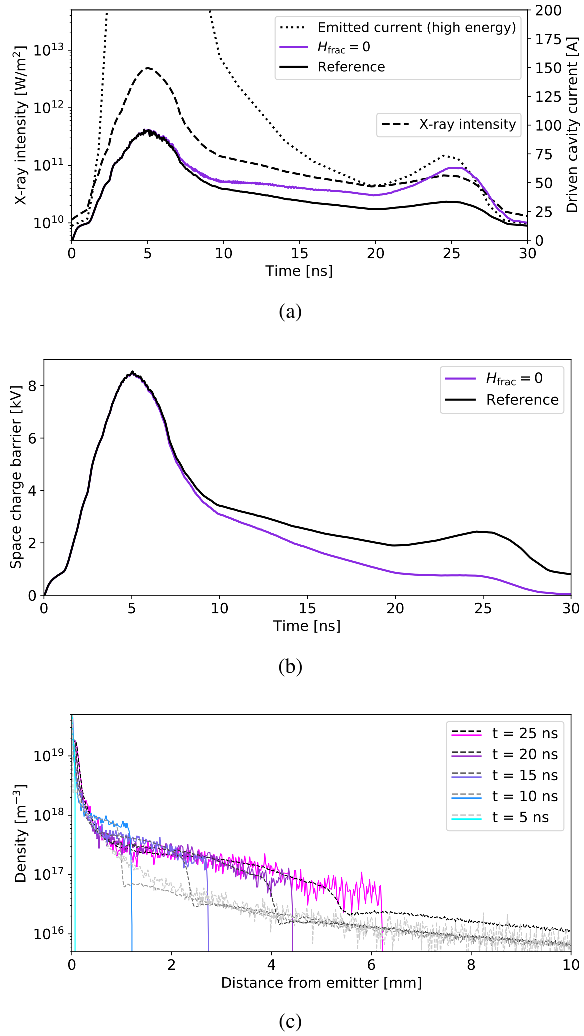

FIG. 4. Results for the reference case and the case with only heavy impurity ions, $H_{\mathrm{frac}} = 0$. The computed cavity currents are plotted in (a). The emitted photocurrent (peak 5.4 kA) and incident x-ray intensity (shown on a log scale) are also plotted in (a) to indicate the magnitude of space charge limiting. Note that the plotted emitted photocurrent quantity only includes the high energy primary and Auger photoelectrons. The space charge barriers are plotted in (b). The space charge barrier is defined to be the minimum value of the electric potential times the charge of an electron. In (c), the evolution of the ion and electron densities over time is shown for $H_{\mathrm{frac}} = 0$. Note that in (c), the electrons are indicated in grayscale and the ions in color.

IV. SUMMARY OF RESULTS AND FURTHER DISCUSSION

The results presented in section III indicate that cavity currents are significantly affected by impurity plasmas. The presence of impurities which contain hydrogen may have a much larger effect on cavity currents compared to impurities which can only lead to the appearance of heavier ions. The structure of computed current waveforms are strongly modified by including an impurity plasma containing hydrogen molecular ions or protons. The reference case, in which no impurity plasma is injected, and the case with only heavy ions exhibit two peaks in the cavity current waveform. Some cases with light ions (protons or hydrogen molecular ions) exhibit a third peak. One of the current peaks will coincide with the stream of light ions reaching the top of the cavity. This peak therefore

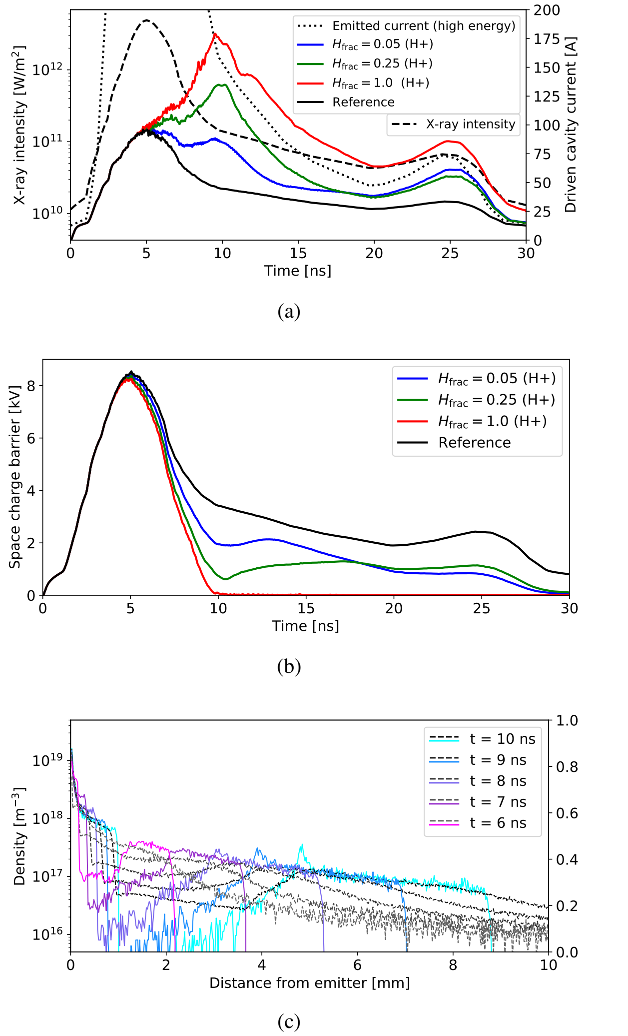

FIG. 5. Results for cases in which light impurity ions of type H+ are injected. The computed cavity currents are plotted in (a), the space charge barriers are plotted in (b) and the evolution of the ion and electron densities, for the $H_{\text{frac}} = 0.25$ case, are shown in (c). A stream of light ions is drawn from the impurity plasma, and the cavity current peak at $t = 10$ ns coincides with the stream of light ions reaching the right of the cavity.

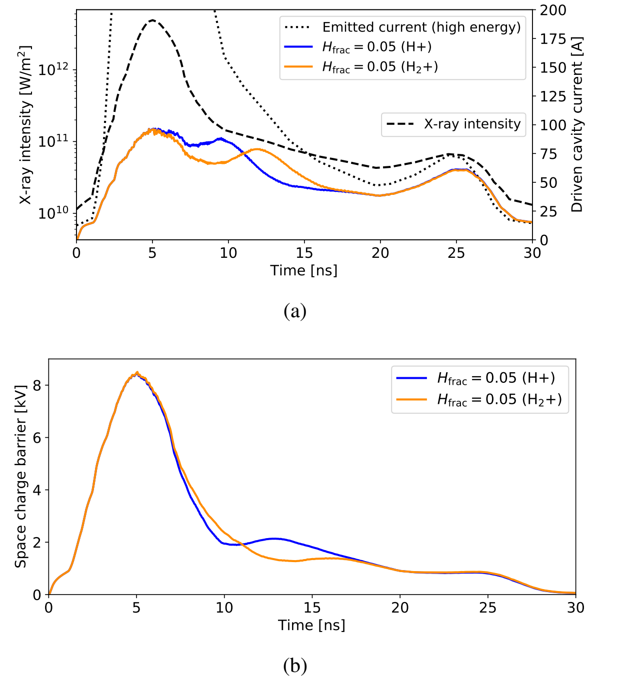

FIG. 6. The result for the case $H_{\text{frac}} = 0.05$ in which light impurity ions of type H_2+ are injected is compared to the case $H_{\text{frac}} = 0.05$ with H+ light ions. An H_2+ ion has twice the mass of an H+ ion. The computed cavity currents are plotted in (a) and the space charge barriers are plotted in (b). The case with H_2+ ions has a cavity current peak at $t = 13$ ns, 2.5 ns later than for the H+ ion case. Correspondingly, the minimum in space charge barrier about occurs 3 ns later for the H_2+ case. This follows from the slower transit time of the more massive H_2+ ions.

occurs slightly later when the impurity plasma contains heavier, less mobile, H_2+ compared to H+. Experimentally, three peaks in the cavity current are often observed when the x-ray intensity has only two peaks. The results presented here may therefore be of use in interpreting the experimental results of x-ray driven cavity experiments.

It is acknowledged that a more sophisticated two- or three-dimensional electromagnetic model will account for phenomena such as electrostatic spreading of the electron beam, magnetic self-pinching and electromagnetic induction. The beam space charge will cause a radial spreading, especially around the edge near $r = 20$ mm. Radial electrostatic spreading may be an important secondary effect in this device. Magnetic self-pinching of a monoenergetic beam will occur if the beam approaches the critical current,

$$I_c = \frac{2\pi r}{\mu_0 e d}\sqrt{2m_e E_0}, \tag{7}$$

where e is the elementary charge, m_e is the mass of an electron, μ_0 is the vacuum permeability and E_0 is the initial electron kinetic energy. This expression is obtained by equating the Larmor radius of an electron at the beam edge to the gap distance d.[28] For $E_0 = 2.8$ keV, which is the mean kinetic energy of the emitted photoelectrons, $I_c = 1.8$ kA. Since the maximum computed cavity current is an order of magnitude smaller than I_c, magnetic self-pinching seems unlikely to be important.

As mentioned in section I, the effect of electromagnetic induction in a somewhat similar problem was explored by Luginsland et al.[4] They found that whether an electrostatic approximation is appropriate or not depends on the rate of injection turn on and the initial kinetic energy of injected electrons. However, there are some significant differences between the present x-ray driven cavity problem and that considered by Luginsland et al. For example, the EEDF is not monoenergetic in the present case. Therefore, in order to gain confidence in the suitability of electrostatics for this problem, some supplementary two-dimensional calculations were undertaken. The emitted photoelectric current and EEDF in these problems are identical to those described above. The results for an electromagnetic model were nearly identical to those obtained using an electrostatic model.

The calculation for the emitter surface temperature indicates a temperature exceeding 3000 K. Since this is well above the boiling temperature for gold at experimental vacuum pressures, ablation of gold metal can be expected. At a pressure of 10 mTorr, the boiling temperature is about 1700 K.[29] Indeed for a shot having a fluence of 15 $\mathrm{kJ/m^2}$, the average intensity is about 3×10^{12} $\mathrm{W/m^2}$ over a 5-ns interval. It is well known that nanosecond laser pulses at this intensity cause significant ablation.[30] Given that the emitter surface will undergo a phase change, there is an open question as to whether thermionic emission of electrons could influence the behavior long after the x-ray intensity becomes small. Further, it is possible that explosive emission of gold droplets and gold ions could be occurring. Vogel and Hoft found that a 20 ns laser pulse having an intensity of 10^{11} $\mathrm{W/m^2}$ can lead to this sort of explosive activity.[31] However the gold ions may be too heavy and immobile to have an effect on the photocurrent of the x-ray driven cavity experiments; this would be consistent with the findings of Weber et al. regarding the effect of tantalum ions in high power diodes. An investigation of these effects and their influence on x-ray driven cavity currents may be of interest in the future.

In this work, an impurity plasma was injected from the emitting surface when the surface temperature would be such that most of the impurities would have desorbed. In future work, it will be of interest to consider a more self-consistent account of impurity plasma formation. For example, using the direct simulation Monte-Carlo method to compute the impact ionization of a desorbed neutral gas. A self-consistent treatment was attempted for inclusion in the present work, but it appeared that a high frequency electrostatic plasma instability occurs and that an implicit time integration method may be required to compute results for such a model. Recently, Rittersdorf et al. discussed some considerations for a self-consistent treatment of electrode plasma formation in high power diodes.[32]

The x-ray cavity model uses a relatively detailed model for the quantum yield of gold, however a blackbody radiation distribution was used for the x-ray energy spectrum. The x-ray spectrum produced by a Z-pinch varies with time throughout the shot and is not necessarily well approximated by a blackbody spectrum at any moment. Future work may benefit from a more realistic x-ray spectrum. However, since the model quantum yield of gold varies by only a factor of three over the entire range of the spectrum considered, it is reasonable to suspect that details in the x-ray spectrum are unlikely to have a very large impact on computed cavity currents.

ACKNOWLEDGMENTS

The author benefited from many valuable discussions with colleagues. He wishes to thank Tim Pointon and Keith Cartwright for thoughtful feedback on this work. He also thanks both of the anonymous referees who provided expert feedback and excellent suggestions during the review process. Sandia National Laboratories is a multimission laboratory managed and operated by National Technology & Engineering Solutions of Sandia, LLC, a wholly owned subsidiary of Honeywell International Inc., for the U.S. Department of Energy's National Nuclear Security Administration under contract DE-NA0003525. This paper describes objective technical results and analysis. Any subjective views or opinions that might be expressed in the paper do not necessarily represent the views of the U.S. Department of Energy or the United States Government.

DATA AVAILABILITY

The data that support the findings of this study are available from the corresponding author upon reasonable request.

[1]K. L. Cartwright, C. H. Moore, N. Roberds, K. S. Bell, T. M. Flanagan, P. J. Christenson, M. T. Bettencourt, T. D. Pointon, D. C. Turner, and E. M. Raybourn, "Initial comparison to experiments of EMPIRE simulations with diodes driven by the photoelectric effect," (International Conference on Numerical Simulation of Plasmas, 2019) SAND2019-10462C.

[2]S. Shields, E. M. Raybourn, K. L. Cartwright, C. H. Moore, N. Roberds, K. S. Bell, T. M. Flanagan, P. J. Christenson, M. T. Bettencourt, and T. D. Pointon, "Initial comparison of EMPIRE simulations with diodes driven by the photoelectric effect," (61st Annual Meeting of the APS Division of Plasma Physics, 2019) pp. NP10–018, SAND2019-12668C.

[3]G. Jaffé, "On the currents carried by electrons of uniform initial velocity," Physical review **65**, 91 (1944).

[4]J. W. Luginsland, S. McGee, and Y. Lau, "Virtual cathode formation due to electromagnetic transients," IEEE transactions on plasma science **26**, 901–904 (1998).

[5]D. Welch, N. Bennett, T. Genoni, D. Rose, C. Thoma, C. Miller, and W. Stygar, "Electrode contaminant plasma effects in 10^7-A Z pinch accelerators," Physical Review Accelerators and Beams **22**, 070401 (2019).

[6]G. Cooperstein, J. Boller, R. Commisso, D. Hinshelwood, D. Mosher, P. Ottinger, J. Schumer, S. Stephanakis, S. Swanekamp, B. Weber, *et al.*, "Theoretical modeling and experimental characterization of a rod-pinch diode," Physics of Plasmas **8**, 4618–4636 (2001).

[7]R. Vesey, T. Pointon, M. Cuneo, T. Mehlhorn, J. Bailey, D. Johnson, and W. Stygar, "Electron–anode interactions in particle-in-cell simulations of applied-B ion diodes," Physics of Plasmas **6**, 3369–3387 (1999).

[8]M. D. Haworth, K. L. Cartwright, J. W. Luginsland, D. A. Shiffler, and R. J. Umstattd, "Improved electrostatic design for MILO cathodes," IEEE transactions on plasma science **30**, 992–997 (2002).

[9]D. Hinshelwood, "Cathode plasma formation in pulsed high current vacuum diodes," IEEE Transactions on Plasma Science **11**, 188–196 (1983).

[10]A. I. Pushkarev and R. V. Sazonov, "Research of cathode plasma speed in planar diode with explosive emission cathode," IEEE transactions on plasma science **37**, 1901–1907 (2009).

[11]I. Langmuir, "The interaction of electron and positive ion space charges in cathode sheaths," Phys. Rev. **33**, 954–989 (1929).

[12]J. Poukey, "Ion effects in relativistic diodes," Applied Physics Letters **26**, 145–146 (1975).

[13]M. Cuneo, "The effect of electrode contamination, cleaning and conditioning on high-energy pulsed-power device performance," IEEE Transactions on Dielectrics and Electrical Insulation **6**, 469–485 (1999).

[14]B. V. Weber, R. J. Allen, B. Moosman, S. J. Stephanakis, F. Young, N. R. Pereira, and J. R. Goyer, "Improved bremsstrahlung from diodes with pulse-heated tantalum anodes," IEEE transactions on plasma science **30**, 1806–1815 (2002).

[15]M. T. Bettencourt, D. A. Brown, K. L. Cartwright, E. C. Cyr, C. A. Glusa, P. T. Lin, S. G. Moore, D. A. McGregor, R. P. Pawlowski, E. G. Phillips, *et al.*, "EMPIRE-PIC: A performance portable unstructured particle-in-cell code," Commun. Comput. Phys. (2021), 10.4208/cicp.OA-2020-0261.

[16]D. Ampleford, "Analysis of Source Data for SATIRE Z shots: Z2234, Z2235, Z2236, Z2237," Tech. Rep. (Sandia National Laboratories, 2011).
[17]E. A. Burke, "Soft X-ray induced electron emission," IEEE Transactions on Nuclear Science **24**, 2505–2511 (1977).
[18]E. Burke and J. Garth, "An algorithm for energy deposition at interfaces," IEEE Transactions on Nuclear Science **23**, 1838–1843 (1976).
[19]F. Biggs and R. Lighthill, "Analytical approximations for X-ray cross sections II," Tech. Rep. (Sandia Laboratories, 1971).
[20]J. Hubbell, P. Trehan, N. Singh, B. Chand, D. Mehta, M. Garg, R. Garg, S. Singh, and S. Puri, "A review, bibliography, and tabulation of k, l, and higher atomic shell X-ray fluorescence yields," Journal of Physical and Chemical Reference Data **23**, 339–364 (1994).
[21]B. L. Henke, J. A. Smith, and D. T. Attwood, "0.1–10-keV x-ray-induced electron emissions from solids—Models and secondary electron measurements," Journal of Applied Physics **48**, 1852–1866 (1977).
[22]C. Mori and T. Watanabe, "Photoelectric emission of metals by X-rays in the keV region," Japanese Journal of Applied Physics **9**, 666 (1970).
[23]B. C. Franke, R. P. Kensek, and T. W. Laub, "ITS version 6: the integrated TIGER series of coupled electron/photon monte carlo transport codes." Tech. Rep. SAND2008-3331 (Sandia National Laboratories, 2008).
[24]N. Roberds, M. T. Bettencourt, K. Cartwright, and C. H. Moore, "A thermal emission injection boundary for plasma simulation." Tech. Rep. (Sandia National Lab.(SNL-NM), Albuquerque, NM (United States), 2019).
[25]D. A. King, "Thermal desorption from metal surfaces: A review," Surface Science **47**, 384–402 (1975).
[26]S. Ramo, "Currents induced by electron motion," Proceedings of the IRE **27**, 584–585 (1939).
[27]P. Virtanen, R. Gommers, T. E. Oliphant, M. Haberland, T. Reddy, D. Cournapeau, E. Burovski, P. Peterson, W. Weckesser, J. Bright, S. J. van der Walt, M. Brett, J. Wilson, K. J. Millman, N. Mayorov, A. R. J. Nelson, E. Jones, R. Kern, E. Larson, C. J. Carey, İ. Polat, Y. Feng, E. W. Moore, J. VanderPlas, D. Laxalde, J. Perktold, R. Cimrman, I. Henriksen, E. A. Quintero, C. R. Harris, A. M. Archibald, A. H. Ribeiro, F. Pedregosa, P. van Mulbregt, and SciPy 1.0 Contributors, "SciPy 1.0: Fundamental Algorithms for Scientific Computing in Python," Nature Methods **17**, 261–272 (2020).
[28]J. Benford, J. A. Swegle, and E. Schamiloglu, *High power microwaves* (CRC press, 2007).
[29]C. Alcock, V. Itkin, and M. Horrigan, "Vapour pressure equations for the metallic elements: 298–2500k," Canadian Metallurgical Quarterly **23**, 309–313 (1984).
[30]J. Ready, *Effects of high-power laser radiation* (Academic Press, 1971).
[31]N. Vogel and H. Hoft, "Cathode spot energy transfer simulated by a focused laser beam," IEEE Transactions on Plasma Science **17**, 638–640 (1989).
[32]I. Rittersdorf, S. Swanekamp, R. Allen, and J. Schumer, "Numerical studies of electrode plasma formation and expansion in high power charged particle beam diodes," in *2014 IEEE 41st International Conference on Plasma Sciences (ICOPS) held with 2014 IEEE International Conference on High-Power Particle Beams (BEAMS)* (IEEE, 2014) pp. 1–4.